Optics Letters

3D trapping of microbubbles by the Marangoni force

J. A. Sarabia-Alonso,[1,*] J. G. Ortega-Mendoza,[2] S. Mansurova,[1] F. M. Muñoz-Pérez,[2] and R. Ramos-García[1]

[1]Departamento de Óptica, Instituto Nacional de Astrofísica, Óptica y Electrónica, Luis Enrique Erro #1, Puebla 72840, Mexico
[2]División de Posgrado, Universidad Politécnica de Tulancingo, Ingenierías #100, Hidalgo 43629, Mexico
*Corresponding author: julio_sarabia21@msn.com

Received 13 August 2021; revised 21 October 2021; accepted 25 October 2021; posted 26 October 2021; published 17 November 2021

In this Letter, we show 3D steady-state trapping and manipulation of vapor bubbles in liquids employing a low-power continuous-wave laser using the Marangoni effect. Light absorption from photodeposited silver nanoparticles on the distal end of a multi-mode optical fiber is used to produce bubbles of different diameters. The thermal effects produced by either the nanoparticles on the fiber tip or the light bulk absorption modulate the surface tension of the bubble wall and creates both longitudinal and transversal forces just like optical forces, effectively creating a 3D potential well. Using numerical simulations, we obtain expressions for the temperature profiles and present analytical expressions for the Marangoni force. In addition, using an array of three fibers with photodeposited nanoparticles is used to demonstrate the transfer of bubbles from one fiber to another by sequentially switching on and off the lasers.

https://doi.org/10.1364/OL.440290

Since the Nobel Laureate Arthur Ashkin *et al*. introduced optical tweezers [1], it triggered a research race for developing and improving non-contact/non-invasive mechanisms not only to trap and manipulate dielectric [2] and metallic [3] particles but also to trap and manipulate biological matter [4].

Even though optical tweezers have extended their landscape of contactless trapping and manipulation, it remains a challenge to trap particles with a refractive index n_p that is smaller than the surrounding medium n_m, i.e., $n_p/n_m < 1$, such as microbubbles [5]. This is due to the repelling optical gradient force that pushes the microbubble out of the high-intensity region of the laser beam [6]. However, this challenge has been faced by several trapping approaches where small bubbles have been 3D trapped using Laguerre-Gaussian beams [7], also called bottle beams, by fast scanning Gaussian-based optical tweezers that act as effective bottle beams [8] and then using ultrashort laser pulses at a high repetition rate [9]. In addition, 2D trapping approaches using optical, convective, and thermocapillary effects have also been implemented but are limited to microbubbles/particles with radii < 10-20 μm [9–11].

Thermocapillary effects have emerged as an efficient and straightforward tool to accomplish non-invasive trapping and 3D manipulation of microbubbles up to 130 μm of radius [12,13]. Moreover, the thermocapillary effect can induce larger and longer-range forces than the optical ones while maintaining the accuracy of the spatial control of the microbubbles [12–18]. Thermophoresis [19–21], which refers to the motion of particles in response to a temperature gradient, has been used to manipulate molecules and even colloidal particles, but to the best of our knowledge it does not apply to bubbles. Optical force magnitude typically lies in the range of fN to pN [10], so trapping large microparticles without damage remains a challenge. In order to trap large objects, several approaches have been demonstrated, such as opto-thermally induced forces, which are many orders of magnitude larger than optical ones [22–24].

In this Letter, we show both 3D steady-state trapping and manipulation of vapor bubbles in liquids using a low-power continuous-wave (CW) laser through the Marangoni effect. Using light absorption from photodeposited silver nanoparticles (AgNPs) on the distal end of an optical fiber or light bulk absorption, we created thermal sources that spatially modulate the surface tension of the bubble wall, creating a longitudinal and transversal force just like optical forces, and effectively creating a 3D potential well. Using numerical simulations, we obtain the expression for the temperature profiles and present an analytical expression for the 3D Marangoni force.

COMSOL Multiphysics software was used to simulate the light absorption at the AgNPs film that were previously photodeposited on the distal end of three different optical fibers using three different lasers ($\alpha_{Ag} = 638.2 \times 10^3\ \mathrm{cm}^{-1}$, $846.3 \times 10^3\ \mathrm{cm}^{-1}$, $871.6 \times 10^3\ \mathrm{cm}^{-1}$ at $\lambda = 445$ nm, 980 nm, and 1550 nm, respectively [25]). Light absorption increases the temperature of the AgNPs, and by heat diffusion, it heats up the surrounding liquid (ethanol) according to the heat transfer equation given by [21]

$$\rho c_p \boldsymbol{u} \cdot \nabla T = \nabla \cdot (\mathrm{K} \nabla T) + Q, \tag{1}$$

where ρ is the ethanol density, c_p is the ethanol heat capacity, $\boldsymbol{u}$ is the field velocity of the fluid, K is the thermal conductivity, $Q = \alpha I_0$ is the heat source per volume unit with α as the absorption coefficient, and I_0 is the optical intensity of the Gaussian beam. Equation (1) assumed a steady-state condition. To model the field velocity of the fluid, i.e., convective currents, the Navier-Stokes equation for incompressible flow, Eqs. (2)

and (3), were coupled to the heat transfer equation and solved by the finite element method

$$\rho\,(\boldsymbol{u}\cdot\nabla)\,\boldsymbol{u}=\nabla\cdot\left\{-p\,\boldsymbol{I}+\mu\left[\nabla\boldsymbol{u}+(\nabla\boldsymbol{u})^{T}\right]\right\}+\boldsymbol{F}_{b}, \quad (2)$$

$$\rho\nabla\cdot\boldsymbol{u}=0, \quad (3)$$

where $\boldsymbol{I}$ is the identity matrix, $\mu = 1.17\times10^{-3}$ Pa·s [12] is the ethanol viscosity, $\boldsymbol{F}_b=-\boldsymbol{g}(\rho(T)-\rho)$ is the volumetric force per volume unit where $\boldsymbol{g}$ is the gravitational acceleration, $\rho(T)$ represents the ethanol density as a function of the temperature, and $\rho = 789\,\mathrm{kg/m^3}$ is the ethanol density at room temperature [13]. The simulation was carried out assuming a 2D configuration, given the problem symmetry. The glass cell possesses rectangular geometry (height 5 mm and width 2 mm). The coordinate system origin is set at the center of the distal end of the optical fiber, as shown in Fig. 1(a). In addition, an initial room temperature (293.15 K) in all boundaries and non-slip boundary conditions were assumed. We model the laser radiation leaving the fiber as a Gaussian beam whose waist ($\omega_0 = 52.5$ μm) corresponds to the core radius of the multimode optical fiber (MMOF) with 15 mW of optical power. Let us consider first that no nanoparticles were photodeposited on the fiber tip and that infrared light ($\lambda = 1550$ nm) propagates along the fiber. In this case, bulk absorption ($\alpha\sim5.63\,\mathrm{cm^{-1}}$) heats up the ethanol and produces a spatially varying temperature distribution. From the COMSOL simulation [see Fig. 1(a)], a Gaussian function and a growth/exponential decay function were found to describe very well the transversal and longitudinal temperature distribution profile, respectively. The transversal temperature profile has the form

$$T_r\,(r,\,z,\,P)=T_0+\Delta T_r\,(z,\,P)\exp\left[-\frac{1}{2}\left(\frac{r}{r_0\,(z,\,P)}\right)^2\right], \quad (4)$$

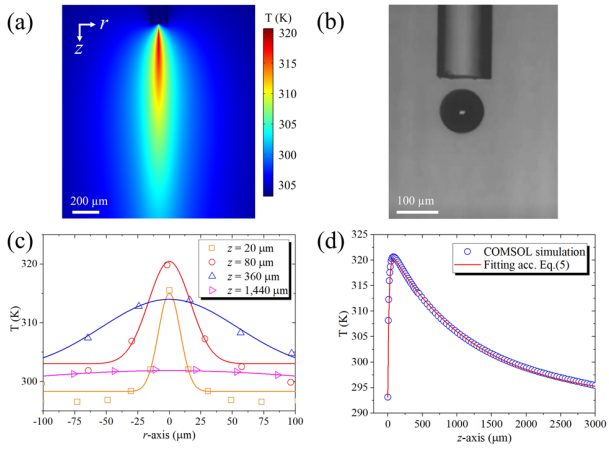

Fig. 1. (a) Temperature distribution in ethanol due to bulk absorption extracted from COMSOL simulations ($\lambda = 1550$ nm and 15 mW of optical power). The scale bar represents 200 μm. (b) 3D trapping and manipulation of a bubble of radius $R = 50$ μm at $\lambda = 1550$ nm and 15 mW. The scale bar represents 100 μm (see Visualization 1). (c) Transversal temperature distribution obtained at different positions along the z-axis. Continuous lines are fit to Gaussian functions in Eq. (4). (d) Longitudinal temperature profile along the propagation axis z. The red line is fitted to Eq. (5).

where r is the transversal radial coordinate, z is the axial coordinate, $\Delta T_r(z,\,P)$ is the temperature difference between the maximum temperature and the offset temperature T_0 (which is approximately the room temperature for mW power levels) and depends on the optical power P and the distance z from the fiber tip, and finally, $r_0(z,\,P)$ is the characteristic distance at which the temperature decays to e^{-1} from its peak.

On the other hand, the longitudinal temperature distribution has the form

$$T_z\,(z,\,P)=T_0+\Delta T_{z1}\,(P)\left(1-\exp\,(-z/z_1)\right)-\Delta T_{z2}\left(1-\exp\,(-z/z_2)\right), \quad (5)$$

where $\Delta T_{z1,2}(P)$ represents the temperature difference between the maximum temperature and the offset temperature T_0, and $z_{1,2}$ are the characteristic distances representing the increase and decrease of the temperature profile. Figures 1(c) and 1(d) show the transversal and longitudinal temperature distribution obtained from COMSOL and the fitting to Eqs. (4) and (5). When absorption from the AgNPs is considered, similar expressions are obtained for the transversal temperature but for the longitudinal one, only the decaying exponential function is present. As can be seen, both equations reproduce the simulated results very well. The temperature distribution discussed above will affect the surface tension of any bubble in the vicinity of the fiber tip and thus will be subject to the Marangoni force $\boldsymbol{F_M}$. This force involves tangential stress on the bubble's wall triggered by the surface tension gradient. The bubble will move towards the zone of the lowest surface tension, i.e., the highest temperature gradient spot. The Marangoni force is given by [12]

$$\boldsymbol{F_M}=-2\pi R^2\nabla T\frac{d\sigma}{dT}, \quad (6)$$

where $d\sigma/dT=-0.1\times10^{-3}\,\mathrm{Nm^{-1}K^{-1}}$ represents the temperature derivative of the ethanol surface tension [12], R is the bubble radius, and ∇T is the temperature gradient. As Eqs. (4) and (5) indicate, there is a radial and longitudinal temperature gradient and therefore a gradient and longitudinal Marangoni force on the bubble given by

$$\boldsymbol{F_{M_r}}=2\pi R^2\frac{d\sigma}{dT}\left(\frac{\Delta T_t\,(z,\,P)}{r_0(z,\,P)^2}\right)r\exp\left[-\frac{1}{2}\left(\frac{r}{r_0\,(z,\,P)}\right)^2\right], \quad (7)$$

$$\boldsymbol{F_{M_z}}=2\pi R^2\frac{d\sigma}{dT}\left\{\left(\frac{\Delta T_{z1}}{z_1}\right)\times\exp\,(-z/z_1)-\left(\frac{\Delta T_{z2}}{z_2}\right)\exp\,(-z/z_2)\right\}. \quad (8)$$

Therefore, 3D trapping of the bubble is expected, as shown in Fig. 1(b). Figure 2(a) shows the transversal Marangoni force $\boldsymbol{F_{M_r}}$ from Eq. (7) taken at $z = 80$ μm, indicating a force profile similar to the optical transversal gradient force, i.e., bubble displacement along $\pm r$ will produce a restoring force directed towards $r = 0$.

Note that the magnitude of both force components depends, among other factors, on the ratio of the temperature increase and the extent of the temperature distribution. Similarly, Fig. 2(b) shows the longitudinal Marangoni force. Note that for

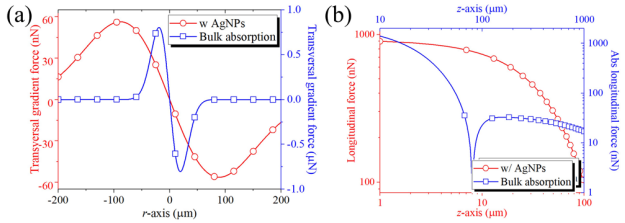

Fig. 2. Marangoni force over a bubble of $R = 50$ μm induced by light bulk absorption of ethanol (blue) and by light absorption from AgNPs photodeposited on the core of an optical fiber (red). (a) Transversal Marangoni force measured at $z = 80$ μm from the fiber tip. (b) Longitudinal Marangoni force.

the bulk absorption, the Marangoni force is negative, i.e., the bubble is being repelled for $z < 80$ μm and attracted for $z > 80$ μm, so the bubble is steadily trapped $z \sim 80$ μm. On the other hand, for AgNPs deposited on the fiber tip, the bubble will always be trapped on the fiber tip. For the bulk absorption the distance where the bubble will be trapped depends on the absorption coefficient. The larger the absorption coefficient, the smaller the distance to the fiber tip. Note that the Marangoni force magnitude lies in the nN-μN range.

The coupling between Eqs. (1)–(3) leads to convective currents, as shown in Fig. 3(a), which in turn results in a drag force $\boldsymbol{F_d} = 6\pi\mu R\boldsymbol{u}(r, z)$, where $\mu = 1.071 \times 10^{-3}$ Pa · s is the dynamic ethanol viscosity [12] and where we emphasize the spatial dependence of the velocity field. It has been proposed that convective currents may exert an additional force that adds up to the trapping force [21]. Similarly, we can decompose the drag force into two orthogonal components: transversal and longitudinal. The transversal force shows similar behavior to the transversal Marangoni force discussed above, so the bubble will be trapped preferably along the propagation distance. Figure 3(c) shows the longitudinal drag force along the z-axis due to the light absorption from AgNPs for a bubble of $R = 50$ μm. Notice that although the fluid velocity magnitude is ∼2 mm/s, the drag force associated with it will produce a maximal force of ∼2 nN directed towards the fiber. Figure 3(d) shows the longitudinal drag force along the z-axis due to the light bulk absorption for the same bubble. Since the longitudinal velocity is directed towards the fiber tip, the drag force will push the bubble towards it.

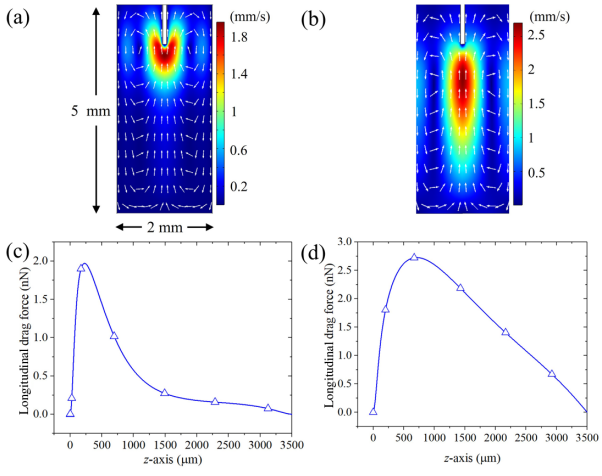

Fig. 3. (a) Convective currents velocity profile due to the light absorption at the AgNPs film ($\lambda = 445$ nm with 10 mW of optical power) extracted from the COMSOL simulations. (b) Convective currents velocity profile due to the light bulk absorption of ethanol ($\lambda = 1550$ nm with 15 mW of optical power) extracted from the COMSOL simulations. (c) Transversal drag force along the z-axis due to light absorption from the AgNPs for a bubble of $R = 50$ μm. (d) Longitudinal drag force gradient along the z-axis due to light bulk absorption of ethanol for a bubble of $R = 50$ μm.

It is well known that a bubble immersed into a liquid will face the buoyancy force $\boldsymbol{F_B} = 4/3\pi\rho_l \boldsymbol{g} R^3$, which always point against the gravity force. In particular, for a microbubble of $R = 100$ μm the buoyancy force is $\boldsymbol{F_B} = 32.4$ nN. The buoyance force increases rapidly as the bubble radius grows and may eventually overcome the Marangoni force and leave the fiber. However, for the microbubbles generated in these experiments, the buoyancy force is smaller than the Marangoni force. Additionally, optical forces may be present, however, since the beam is not strongly focused (9 μm for single-mode fiber and 105 μm for multi-mode optical fibers). Both the gradient and the force associated with the radiation pressure lies in the range of pN, which is much smaller than the Marangoni, drag, and buoyancy force. For such reasons, optical forces will not be considered in this analysis.

Figure 4(a) shows the transversal force components at $z = 100$ μm of the optothermal forces ($\boldsymbol{F_M}$, $\boldsymbol{F_d}$) acting on a microbubble of $R = 100$ μm induced by the light absorption at the AgNPs. As noted before, the transversal component of both the Marangoni and the drag force acts as an attractive force and endorses bubble trapping. In addition, the maximal transversal Marangoni gradient force is ∼250 times larger than the velocity–associated drag force. Figure 4(b) shows the longitudinal components of the Marangoni, drag, and buoyancy force. Likewise, the longitudinal Marangoni force dominates over the other components near the fiber end, but far away from the fiber end, the buoyancy force dominates.

Since the Marangoni force is much larger than the buoyancy force, a microbubble can, in principle, be trapped in a horizontal plane. In fact, we found that by placing three different optical fibers (one multi-mode for microbubble generation and two single-mode for trapping) in a horizontal plane, a microbubble can be trapped and transferred from one fiber to the next by sequentially switching on and off the CW lasers, as shown in Fig. 5 and Visualization 2. The microbubble was generated by evaporating the ethanol in contact with AgNPs that were previously photodeposited [26] on one end of the multi-mode optical fiber (OF_1) with an internal and external diameter of 105/125 μm, respectively. Light from a CW laser emitting at 445 nm (BWTEK model BWF1-445-450) and propagating

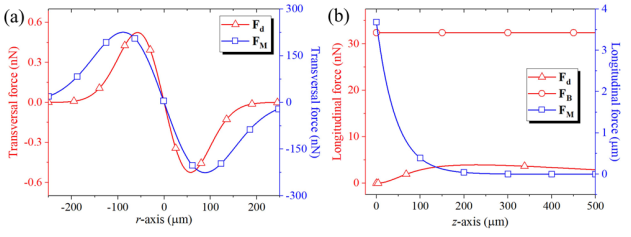

Fig. 4. Optothermal forces on a microbubble of $R = 100$ μm. (a) Transversal components of the gradient forces $\mathbf{F_d}$ (red triangles) and $\mathbf{F_M}$ (blue squares). (b) Longitudinal component of $\mathbf{F_M}$ (blue squares), $\mathbf{F_d}$ (red triangles), and $\mathbf{F_B}$ (red dots). Since $\mathbf{F_M} \gg \mathbf{F_d}$ and $\mathbf{F_B}$, the microbubble is attracted to the optothermal source, i.e., the distal end of the optical fiber.

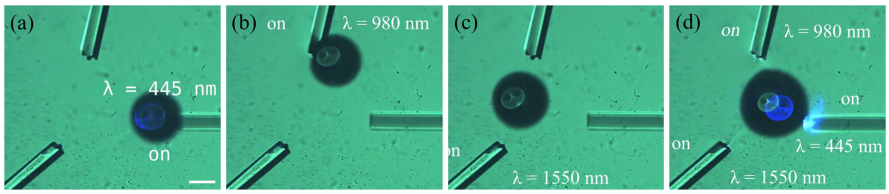

Fig. 5. Trapping and manipulation of a microbubble of $R = 100$ μm by optothermal effects induced at a different wavelength with low optical powers. The microbubble is photothermally generated by the CW laser at 445 nm with 13 mW (not shown). (a) Only the CW laser at 445 mW is turned on, inducing the microbubble trapping by the MMOF (OF_1). The scale bar represents 200 μm. (b) The CW laser at 445 nm is turned off and only the CW laser at 980 nm is turned on, inducing the microbubble displacement towards the single-mode optical fiber (SMOF) (OF_2). (c) The CW laser at 980 nm is turned off and only the CW laser at 1550 nm is turned on, inducing the microbubble displacement towards the SMOF (OF_3). (d) The three CW lasers are turned on, trapping the microbubble at the center of the optical fiber array (see Visualization 2).

through the OF_1 was used to heat up the AgNPs and evaporate the liquid. Two additional single-mode fibers (OF_2 and OF_3, 9/125 μm) also with previously photodeposited AgNPs were coupled to two CW lasers emitting 980 nm (Thorlabs model BL976-SAG300, 5 mW) and 1550 nm (Thorlabs model SFL-1550S, 4 mW). The distal ends of the three optical fibers were immersed in a glass cell filled with pure ethanol and separated ∼ 800 μm from each other, as it is shown in Fig. 5. The temperature reached at the interface is a function of both the laser power P and the silver absorption coefficient α_{Ag} at the wavelength employed, so the interface temperature can be raised beyond the boiling point of the ethanol (∼78 °C) [12]. To visualize the generation and manipulation of the bubble a 5× microscope objective was used and a Motic3 camera (3 Mpx resolution) was connected to a computer. The illumination was provided by a white lamp. Note that the bubble is out of focus, which means that the buoyancy force moves the bubble out of the plane of the trapping fibers. The Marangoni force is so strong that one can see the bubble deformation when the laser is turned on. Moreover, since the absorption from the AgNPs is large in the visible and NIR, our experimental results show that there is no spectral selectivity in the trapping and 3D manipulation of microbubbles by the Marangoni effect, i.e., the microbubble is trapped and manipulated by CW lasers emitting at different wavelengths with low optical powers.

In conclusion, we have demonstrated, both theoretically and experimentally, the 3D trapping and manipulation of photothermally induced microbubbles by the Marangoni force. As in optical tweezers, Marangoni and drag forces can be decomposed in transversal and longitudinal gradient force components. The maximal longitudinal gradient force is achieved on the surface of the fiber if nanoparticles are photodeposited. In the case of light bulk absorption in ethanol, the bubble is trapped at ∼80 μm from the fiber tip (for $\lambda = 1550$ nm and $\alpha \sim 5.63\ \mathrm{cm}^{-1}$). Although drag (generated by convective currents) and buoyancy forces are present, they are much smaller than the Marangoni one. Finally, we show that a bubble can be displaced from one fiber to another by sequentially switching the light sources. 3D trapping of large bubbles opens the opportunity for more complex manipulation configurations.

Funding. Consejo Nacional de Ciencia y Tecnología (grant 261148, OISE:PIRE-SOMBRERO)/(CONACyT 251992).

Disclosures. The authors declare no conflicts of interest.

Data Availability. Data underlying the results presented in this Letter are not publicly available at this time but may be obtained from the authors upon reasonable request.

REFERENCES

1. A. Ashkin, J. M. Dziedzic, J. E. Bjorkholm, and S. Chu, Opt. Lett. **11**, 288 (1986).
2. D. Gao, W. Ding, M. Nieto-Vesperinas, X. Ding, M. Rahman, T. Zhang, C. Lim, and C.-W. Qiu, Light Sci. Appl. **6**, e17039 (2017).
3. K. Svoboda and S. M. Block, Opt. Lett. **19**, 930 (1994).
4. F. M. Fazal and S. M. Block, Nat. Photonics **5**, 318 (2011).
5. H. Takahira, M. Shirasawa, and S. Yamasaki, JSME Int. J. **43**, 393 (2000).
6. A. Ashkin, Biophys. J. **61**, 569 (1996).
7. P. A. Prentice, M. P. MacDonald, T. G. Frank, A. Cuschieri, G. C. Spalding, W. Sibbett, P. A. Campbell, and K. Dholakia, Opt. Express **12**, 593 (2004).
8. T. J. Smart, M. B. Unlu, and P. H. Jones, Proc. SPIE **10347**, 1034731 (2017).
9. S. V. Oshemkov, L. P. Dvorkin, and V. Y. Dmitriev, Tech. Phys. Lett. **35**, 282 (2009).
10. B. L. Lü, Y. Q. Li, H. Ni, and Y. Z. Wang, Appl. Phys. B **71**, 801 (2000).
11. J. Y. Ye, G. Chang, T. B. Norris, C. Tse, M. J. Zohdy, K. W. Hollman, M. O'Donnell, and J. R. Baker, Jr., Opt. Lett. **29**, 2136 (2004).
12. J. A. Sarabia-Alonso, J. G. Ortega-Mendoza, J. C. Ramírez-San-Juan, P. Zaca-Morán, J. Ramírez-Ramírez, A. Padilla-Vivanco, F. M. Muñoz-Pérez, and R. Ramos-García, Opt. Express **28**, 17672 (2020).
13. J. G. Ortega-Mendoza, J. A. Sarabia-Alonso, P. Zaca-Morán, A. Padilla-Vivanco, C. Toxqui-Quitl, I. Rivas-Cambero, J. Ramirez-Ramirez, S. A. Torres-Hurtado, and R. Ramos-Gracía, Opt. Express **26**, 6653 (2018).
14. A. Miniewicz, C. Quintard, H. Orlikowska, and S. Bartkiewicz, Phys. Chem. Chem. Phys. **19**, 18695 (2017).
15. Y. Li, U. Abeywickrema, and P. Banerjee, Opt. Eng. **58**, 084107 (2019).
16. O. V. Angelsky, A. Ya. Berkshaev, P. P. Maksimyak, and A. P. Maksimyak, and S. G. Hanson, Opt. Express **26**, 13995 (2018).
17. N. A. Ivanova and B. A. Bezuglyĭ, Tech. Phys. Lett. **32**, 854 (2006).
18. F. M. Muñoz-Pérez, J. G. Ortega-Mendoza, A. Padilla-Vivanco, C. Toxqui-Quitl, J. A. Sarabia-Alonso, and R. Ramos-García, Front. Phys. **8**, 585590 (2020).
19. S. Duhr and D. Braun, Phys. Rev. Lett. **97**, 038103 (2006).
20. Y. Shi, T. Zhu, T. Zhang, A. Mazzulla, D. P. Tsai, W. Ding, A. Q. Liu, G. Cipparrone, J. J. Sáenz, and C.-W. Qiu, Light Sci. Appl. **9**, 62 (2020).
21. J. A. Zenteno-Hernandez, J. Vázquez Lozano, J. A. Sarabia-Alonso, J. Ramírez-Ramírez, and R. Ramos-García, Opt. Lett. **45**, 3961 (2020).
22. J. Li and Y. Zheng, Acc. Mater. Res. **2**, 352 (2021).
23. L. Lin, E. H. Hill, X. Peng, and Y. Zheng, Acc. Chem. Res. **51**, 1465 (2018).
24. C. Zhao, Y. Xie, Z. Mao, Y. Zhao, J. Rufo, S. Yang, F. Guo, J. D. Mai, and T. J. Huang, Lab Chip **14**, 384 (2014).
25. Y. Jiang, S. Pillai, and M. A. Green, Sci. Rep. **6**, 30605 (2016).
26. J. G. Ortega-Mendoza, F. Chávez, P. Zaca-Morán, C. Felipe, G. F. Pérez-Sánchez, G. Beltran-Pérez, O. Goiz, and R. Ramos-García, Opt. Express **21**, 6509 (2013).